Rev. Roum. Sci. Techn.– Électrotechn. et Énerg.
Vol. **71**, *2*, pp. 317–322, Bucarest, 2026

STUDIES ON THE DESIGN AND ANALYSIS OF SLOT-LOADED PATCH ANTENNA FOR X-BAND APPLICATIONS

GOPINATH DHAMOTHARAKANNAN[1], MARICHAMY PERUMALSAMY[2]

Keywords: Antenna; Defected ground structure; FR-4 substrate; Slot antenna; X-band.

In this article, a miniaturized square slot-loaded patch antenna with a rectangular bulged slot and a complementary π-shaped slot carved on the ground plane is proposed. The tri-band of resonant frequencies was obtained by exciting a rectangular bulged slot and a complementary π-shaped slot with a microstrip-fed slot-loaded patch antenna. FR-4 dielectric substrate of 50 mm x 50 mm x 1.56 mm has been used to fabricate the antenna. The resonant frequencies of 8.4, 9.4, and 11.9 GHz were acquired for X-band applications, including wireless networks, radar systems, and satellite communications. Impedance matching and wide bandwidth are achieved with the implementation of the defected ground structure (DGS) technique. The experimental validation of antenna characteristics, including reflection coefficient, gain, bandwidth, and radiation efficiency, demonstrates strong concordance with simulated results.

1. INTRODUCTION

The X-band (8–12 GHz) region of the microwave spectrum is widely employed in applications such as radar systems, satellite communications, point-to-point links, air traffic control and surface movement radar, synthetic aperture radar (SAR), and television broadcasting. In biomedical electromagnetics, this frequency band supports medical imaging techniques, including microwave tomography for breast cancer diagnosis and dielectric imaging for tissue characterization [1–3]. X-band microwave systems are being utilized in healthcare applications, including hyperthermia-based cancer therapy, biotelemetry, non-invasive blood glucose monitoring, endoscopic imaging, bone and joint imaging, and respiration monitoring.

For X-band applications, prominent antenna types include microstrip patch, horn, parabolic reflector, and slot antennas, each selected based on criteria such as gain, radiation pattern, polarization, and physical limitations [4,5]. Key design factors for X-band antennas include compact size, high radiation efficiency, and adequate impedance bandwidth. Multiband slot- and patch-based antennas are particularly attractive due to their low-profile design, ease of fabrication, and capacity for wideband operation across multiple frequency bands [6,7].

Microstrip antennas are extensively utilized in contemporary wireless and microwave communication systems owing to their planar structure and compatibility with integrated circuit technology. However, conventional microstrip antennas exhibit limitations, including narrow bandwidth, low radiation efficiency, spurious radiation, and challenges in achieving high gain and polarization purity. Design methodologies, including slot loading and defective ground structures, have been proposed to mitigate these drawbacks, though they often increase design complexity and involve performance trade-offs [8–10].

Various antenna designs have been proposed for X-band and related applications. In [11,12], rectangular microstrip antennas with defected ground structures or partially reflecting surfaces achieved wide bandwidths and moderate gains. Meta-surface-based slot-notched patch antennas have been designed for dual-band function [13], while self-triplexing antennas utilizing nonlinear hybrid slots and substrate-integrated waveguides have enabled multi-frequency operation with improved port isolation [14]. Other designs include dual-polarization reconfigurable monopole antennas [15], aperture antenna arrays for synthetic aperture radar [16], and compact circularly polarized multiband antennas with split-ring resonators [17]. These designs indicate advancements in bandwidth, polarization, and gain, but many are limited to single- or dual-band operation or require complex structures such as AMCs and SIWs, increasing design and fabrication challenges.

This study introduces a low-profile square patch antenna featuring a rectangular bulged slot and a complementary π-shaped slot etched on the ground plane. The antenna operates at three frequency bands, and a partial ground plane (PGP) is utilized to improve gain and radiation efficiency. The novelty of the design lies in realizing triple-band operation in a compact, low-profile structure with high gain and efficiency, without relying on complex AMC or SIW configurations, making it suitable for X-band applications. The antenna is fabricated on an FR-4 substrate for its low cost and availability; although its higher dielectric loss can slightly reduce gain and efficiency, design features such as the PGP and slot loading mitigate these effects, ensuring acceptable X-band performance.

2. ANTENNA DESIGN

Figure 1 shows the geometric specification of the antenna. The antenna is made on an FR-4 substrate with a dielectric constant (ε_r) of 4.4, height of the substrate (h) of 1.56 mm, and a loss tangent (tan δ) of 0.02. Figure 1a illustrates the top view of the antenna. The physical dimensions are initially determined using resonant frequency and the antenna design equations outlined in [18–20]. The antenna's physical parameters are specified in Table 1.

Table 1

Antenna physical parameters.

Physical Parameters	Dimensions [mm]
Ground plane and Patch length (L)	50
Ground plane and Patch width (W)	50
Square Slot Length (sL)	33.8
Square Slot Width (sW)	33.8
Ground slot length (g1L)	23
Ground slot width (g1W)	8
π shaped slot length (g2L)	6.5
π shaped slot width (g2W)	7
Complementary π shaped slot length (g3L)	4
Complementary π shaped slot width (g3W)	5
Thickness of the Substrate (h)	1.56

A square slot is loaded into the patch to reduce the effective radiating area and improve the antenna's radiation characteristics, such as reflection coefficient, bandwidth,

[1] Department of ECE, Ramco Institute of Technology, Rajapalayam, Tamil Nadu, India-626117. E-mail: gopinath@ritrjpm.ac.in
[2] Department of ECE, P.S.R Engineering College, Sivakasi, Tamil Nadu, India-626140. E-mail: pmarichamy@psr.edu.in

DOI: 10.59277/RRST-EE.2026.2.25

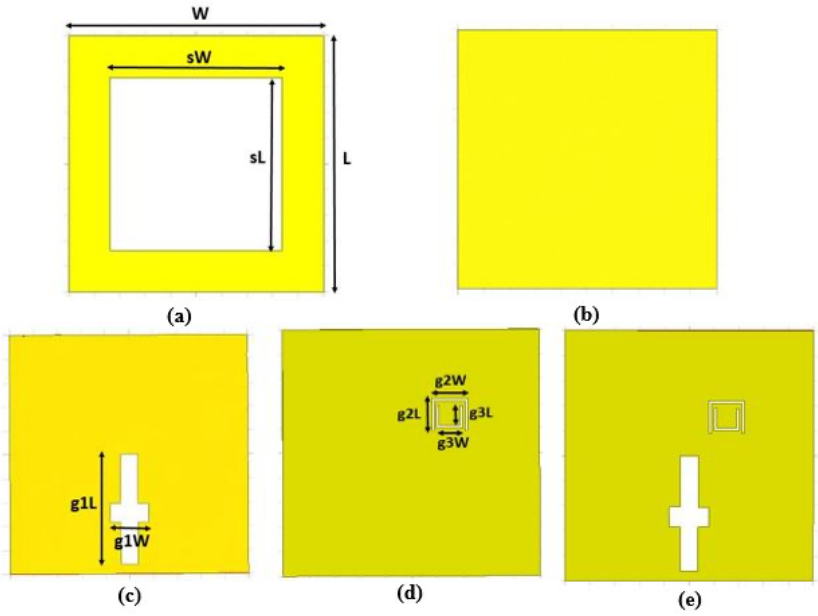

Fig. 1 – The geometrical details of the antenna: (a) Top view; (b) Full ground plane-bottom view (stage I); (c) Rectangular bulged slot (stage II); (d) Complementary π-shaped slot (stage III), and (e) Final ground plane (stage IV).

gain, radiation efficiency, *etc*. Initially, the size of the square slot is 33 mm × 33 mm. In Stage I, the full ground plane is utilized, as shown in Fig. 1.

2.1 ANALYSIS OF ANTENNA

By varying the square slot side length (sL) from 33 mm to 34 mm with a period of 0.2 mm, six reflection coefficient responses were obtained using the parametric analysis method in HFSS. From Fig. 2, the optimized square slot side length (sL) of 33.8 mm was obtained for three resonating frequencies of 8.4, 9.4, and 11.9 GHz. Reflection coefficients of -40, -22, and -19 dB were observed at 8.4, 9.4, and 11.9 GHz, respectively. To improve antenna characteristics, such as the reflection coefficient, gain, bandwidth, and radiation efficiency, the ground plane is further modified.

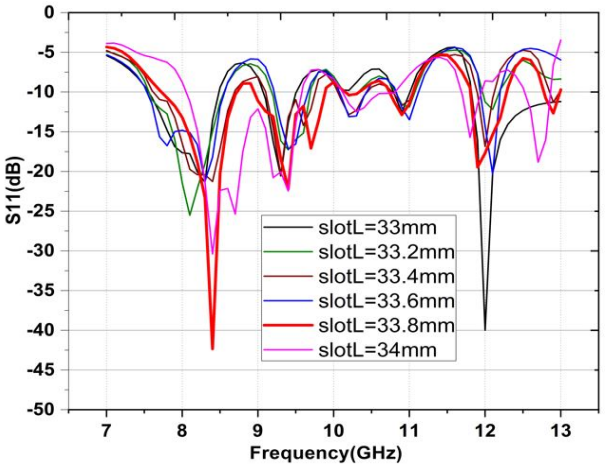

Fig. 2 – Parametric analysis of square slot length.

In stage II, a rectangular bulged slot is incorporated into the antenna's ground plane. The dimensions of the rectangular bulged slot are 23 mm and 8 mm. Simulated reflection coefficients of -15, and -17 dB are obtained at 8.4 and 11.8 GHz. The reflection coefficient for stage II is shown in Fig. 3.

In stage III, a complementary π-shaped slot is extracted from the ground plane after the rectangular bulged slot is removed. The dimensions of the π-shaped slot are g2L = 6.5 mm, g2W = 7 mm, g3L = 4 mm, and g3W = 5 mm. The stage III defective ground structure is shown in Fig. 1d. After etching the complementary π-shaped slot, the simulated reflection coefficient was obtained in the HFSS tool. Reflection coefficients of -18, -17, and -16.5 dB were observed at 8.4, 9.4, and 11.8 GHz, respectively. From the graph, the bandwidth is narrowed.

In stage IV, the rectangular bulged slot and the complementary π-shaped slot are etched from the ground plane. The simulated reflection coefficient of stage IV is shown in Fig. 3. From the graph, it is evident that the reflection coefficient is improved for all three resonating frequencies. Reflection coefficients of -42, -32, and -26 dB are obtained at 8.4, 9.4, and 11.9 GHz, respectively. The bandwidth is also improved.

The 3D radiation pattern was simulated at 8.4 GHz and exhibits a stable, well-defined broadside response with a peak gain of 6.94 dBi, and it is shown in Fig. 4. The smooth, symmetric pattern with low side-lobes and suppressed back radiation, enabled by the slot-loaded patch and defected ground structure, confirms proper mode excitation and good impedance matching.

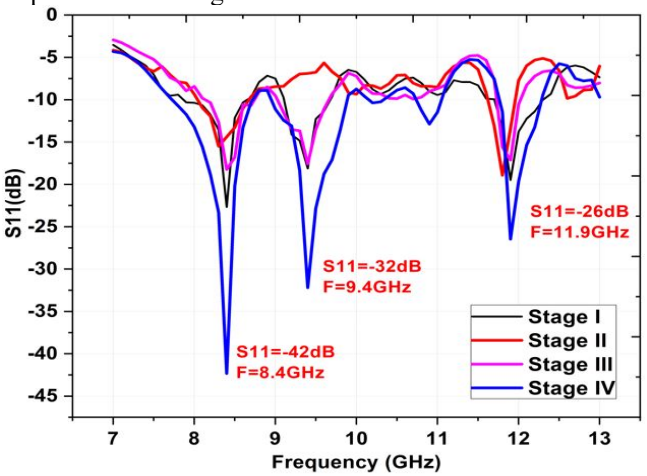

Fig. 3 – Reflection coefficient of different stages of antenna design.

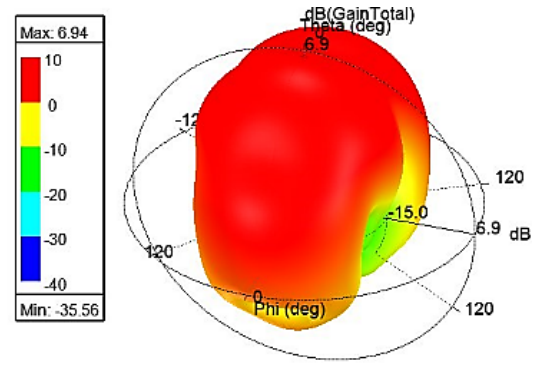

(a) 8.4 GHz

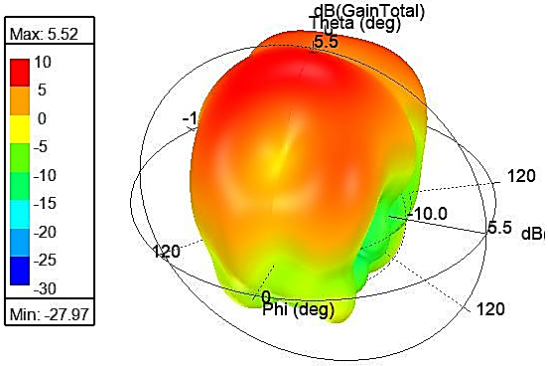

(b) 9.4 GHz

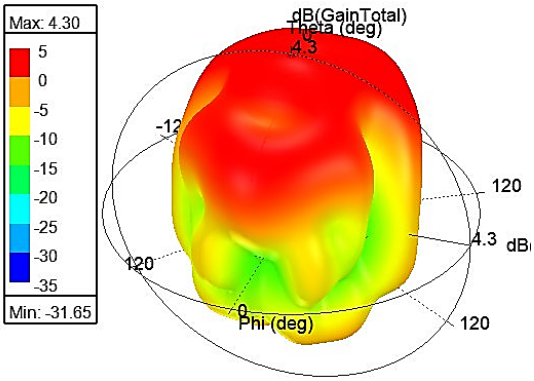

(c) 11.9 GHz

Fig. 4 – 3D radiation pattern at different resonating frequencies.

At 9.4 GHz, the 3D radiation pattern indicates a well-defined broadside beam with a peak gain of 5.52 dBi. The pattern is smooth with moderate symmetry, and side-lobe levels are controlled, while back radiation is slightly higher. These properties indicate effective excitation of the resonant mode, efficient radiation, and good impedance matching.

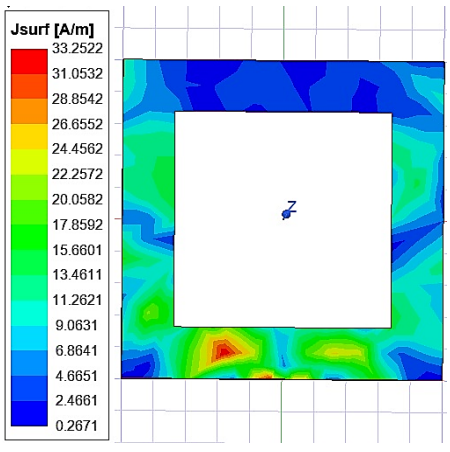

(a) 8.4 GHz.

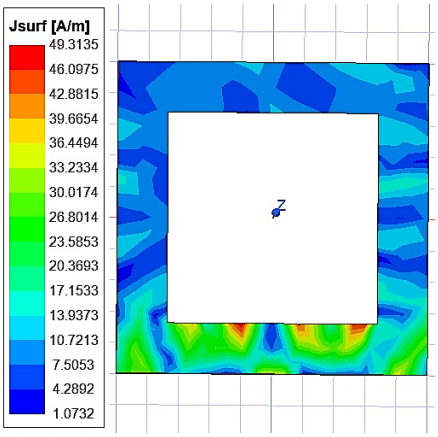

(b) 9.4 GHz.

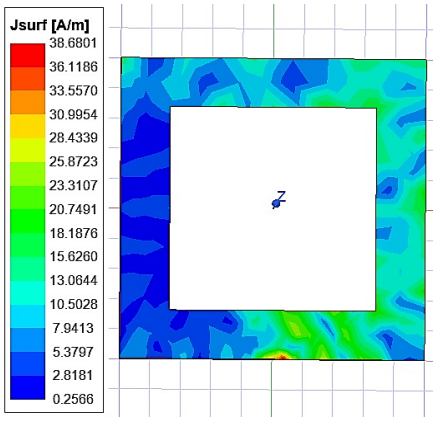

(c) 11.9 GHz.

Fig. 5 –Surface current distributions

At 11.9 GHz, the 3D radiation pattern exhibits a consistent broadside beam with a peak gain of 4.30 dBi. The pattern shows slight spreading and minor asymmetry, typical of higher-order resonances. Side-lobes and back radiation are moderately increased compared to lower bands, yet the overall radiation remains well-controlled, confirming effective mode excitation and acceptable directional performance.

The surface current distributions at 8.4, 9.4, and 11.9 GHz indicate edge and slot-dominated higher-order resonant behavior, as shown in Fig. 5. At 8.4 GHz, currents are concentrated along the edges and corners of the square aperture, with weak central excitation, indicating multimodal, edge-driven resonance. At 9.4 GHz, enhanced currents along the lower edge and adjacent corners indicate stronger field localization and frequency-selective radiation, while the central region remains predominantly inactive. At 11.9 GHz, currents are concentrated along the patch edges and slot boundaries, with weak central currents, confirming a slot-induced higher-order hybrid mode. Across all three frequencies, these distributions show that edge geometry, slot configuration, and boundary discontinuities significantly influence resonance, impedance matching, and radiation efficiency of the antenna.

3. RESULTS AND DISCUSSIONS

The antenna was fabricated, and with the help of a Keysight network analyzer, the reflection coefficient was measured. Fig. 6 shows the top and bottom views of the fabricated antenna. The measured and simulated reflection coefficients of three resonating frequencies are compared in

Fig. 5. Reflection coefficients of -36, -17, and -15 dB were measured at 8.4, 9.4, and 11.8 GHz, respectively.

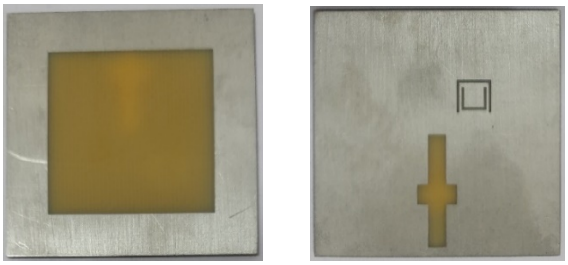

Fig. 6 – Fabricated Antenna top view and bottom view.

Compared to the simulated results, measured reflection coefficients were degraded for all the resonating frequencies. The measured impedance bandwidths are also mentioned in Fig. 7. The -10 dB impedance bandwidths obtained are 0.4 GHz (8.6-8.2 GHz, centered at 8.4 GHz), 0.5 GHz (9.7-9.2 GHz, centered at 9.4 GHz), and 0.2 GHz (12-11.8 GHz, centered at 11.9 GHz).

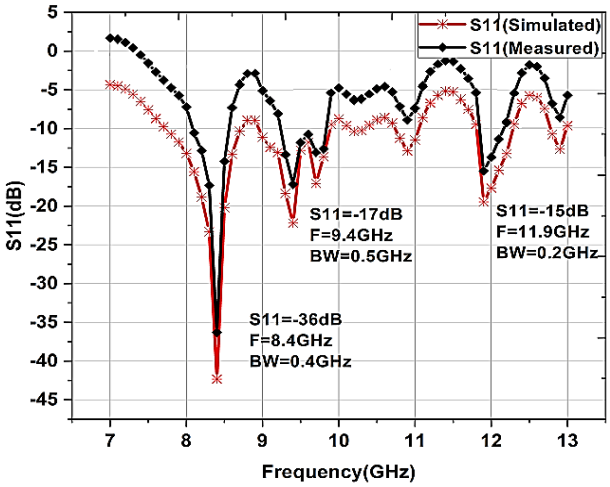

Fig. 7 – Comparative view of measured and simulated reflection coefficient.

The 2D radiation pattern is simulated using the HFSS tool. The E-plane and H-plane patterns were simulated with $\varphi = 0^0$ and $\theta = 90^0$, respectively, and are shown in Fig. 8. The fabricated antenna was placed in the anechoic chamber with a proper implementation setup.

Then, the 2D radiation pattern was measured at the triband frequencies and is shown in Fig. 8. Compared to the simulated radiation pattern, the measured radiation pattern is slightly degraded due to substrate losses, fabrication tolerances, and connector and soldering effects.

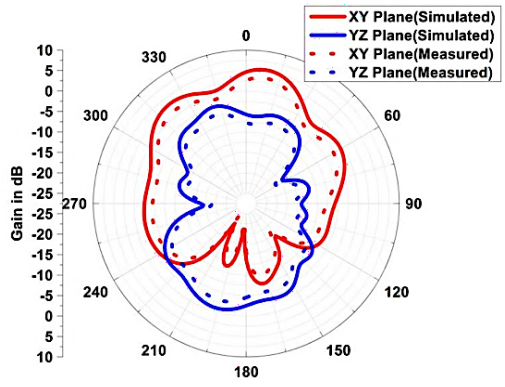

(a) 8.4 GHz.

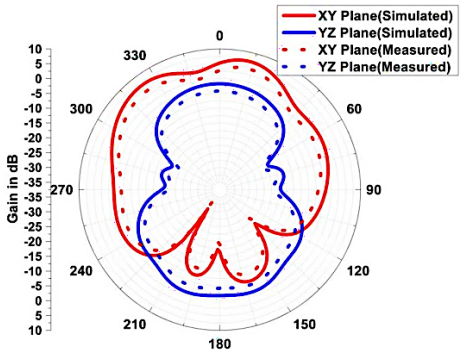

(b) 9.4 GHz

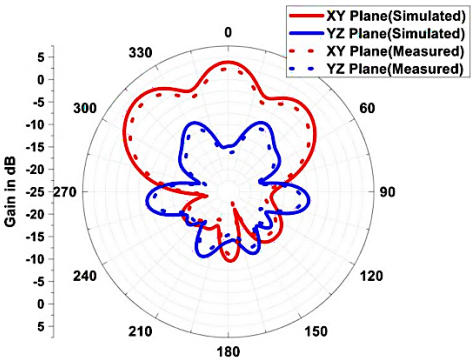

(c) 11.9 GHz.

Fig. 8 – 2D radiation pattern at different resonating frequencies.

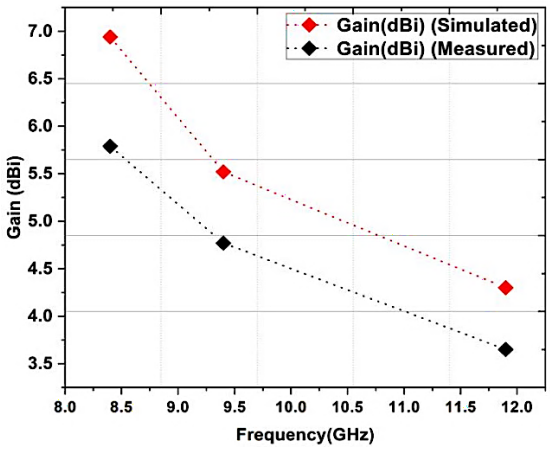

Fig. 9 – The comparison of simulated and measured gain.

The gain is simulated using HFSS, and the values are 6.94, 5.52, and 4.30 dBi at 8.4, 9.4, and 11.9 GHz, respectively. The antenna's radiation efficiency and gain were measured. Fig. 9 shows a comparison of the measured and simulated gains. The antenna's measured gain is 5.79, 4.77, and 3.65 dBi at 8.4, 9.4, and 11.9 GHz, respectively. Compared to the simulated gain, the measured gain was decreased due to dielectric losses and SMA connector losses. The radiation efficiencies of 93%, 86%, and 82% were obtained at 8.4, 9.4, and 11.9 GHz, respectively. The radiation efficiency as a function of frequency is shown in Fig. 10.

This antenna design exhibits a well-balanced performance compared with recently reported antennas in the literature, as shown in Table 2. Previous works primarily emphasize single- or dual-band operation with either narrow bandwidths or higher design complexity. Although certain designs attain considerable gain or wideband performance, they frequently have minor fluctuations in efficiency or increased design complexity.

Table 2
Comparison of the proposed antenna with other antennas.

Ref. & Year	Frequency (GHz)	Bandwidth (GHz)	Reflection Coefficient (dB)	Gain (dBi)	Radiation Efficiency (%)	Design complexity
[13] & 2023	(8.11-11.14)	3.03	-32	8.72	91	High
[15] & 2023	(9.88-11.06)	1.18	-24	5.71	-	High
[16] & 2023	5.35, 9.65	0.065, 0.354	-32	13.2,10.6	-	Low
[7] & 2024	(2.8-3.2), (6.16-10.45)	0.4,4.4	-22,-24	5.8	80	Moderate
[22]& 2024	2.45,5.85,8.83	0.1,0.7,1.8	-12,-20,-24	2.75, 3.53, 4.36	77,82,84	Moderate
[21] & 2025	5.7,9.5	0.31,0.5	-31	7.2,5.8	-	High
[19] & 2025	9.5	0.4	-35.84	6.35	-	High
Proposed Antenna	8.4, 9.4, 11.9	0.4,0.5,0.2	-36, -17, -15	6.94, 5.52, 4.30	93, 86, 82	Low

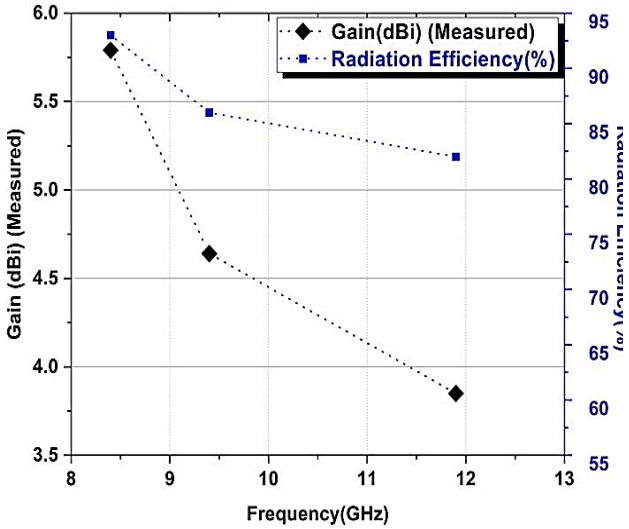

Fig. 10 – Measured gain and radiation efficiency of the antenna.

The antenna functions at three resonant frequencies (8.4, 9.4, and 11.9 GHz) with acceptable impedance bandwidths and good reflection coefficients (-36, -17, and -15 dB). It exhibits competitive gain (up to 6.94 dBi) as well as high radiation efficiency (86–93%) while preserving low design complexity, rendering it a preferable alternative to the present systems.

4. CONCLUSIONS

A slot-loaded patch antenna resonates at a triband of frequencies in the X band and gives better gain and bandwidth, along with high radiation efficiency. The rectangular bulged slot and a complementary π-shaped slot are extracted from the ground plane. The antenna parameters are validated experimentally, and it is fit for X-band applications. In the future, the polarization and diversity of the antenna will be investigated with the parameter of axial ratio. The integration of advanced materials and fabrication methods further enhances the feasibility of the proposed slot-loaded patch antenna, allowing for greater versatility in deployment across different platforms and environments.

ACKNOWLEDG(E)MENT(S)

The authors thank Ramco Institute of Technology for providing them with all the amenities and opportunities to successfully complete the model, as well as for providing space to share their ideas with the research community.

CREDIT AUTHORSHIP CONTRIBUTION STATEMENT

GOPINATH DHAMOTHARAKANNAN worked on methodology, design concept, Antenna analysis, simulations, measurements, and writing of the paper.

MARICHAMY PERUMALSAMY has supervised the work and simulation as well as reviewed the manuscript.

Received on 02 January 2026

REFERENCES

1. Y.-H. Yang, B.-Y. Liu, S.-G. Zhou, *A wideband cavity-backed dual-polarized antenna for X-band applications*, IEEE Antennas and Wireless Propagation Letters, **22**, *4*, pp. 913–917 (2023).
2. M.E. Hammoumi, F. Tubbal, N.E.A.E. Idrissi, P.I. Theoharis, S. Abulgasem, R. Raad, *A wideband circularly polarized CPW-fed printed monopole X-band antenna for CubeSat applications*, IEEE Access, **11**, pp. 121077–121086 (2023).
3. E. Arnaud et al., *Compact isoflux X-band payload telemetry antenna with simultaneous dual circular polarization for LEO satellite applications*, IEEE Antennas and Wireless Propagation Letters, **19**, *10*, pp. 1679–1683 (2020).
4. G. Rajesh, R. Poonkuzhali, *Design and analysis of CPW-fed ultrathin flexible MIMO antenna for UWB and X-band applications*, IEEE Access, **12**, pp. 96704–96717 (2024).
5. M.A. Belen, F. Güneş, A. Çalışkan, P. Mahouti, S. Demirel, A. Yıldırım, *Microstrip SIW patch antenna design for X band application*, Proc. 21st Int. Conf. Microwave, Radar Wireless Commun. (MIKON), Kraków, Poland, pp. 1–3 (2016).
6. M.V. Yadav, S.V. Yadav, T. Ali, S.K.K. Dash, N.T. Hegde, V.G. Nair, *A cutting-edge S/C/X band antenna for 5G and beyond application*, AIP Advances, **13**, *10*, pp. 1–10 (2023).
7. A. Unal, T.S. Delwar, P. Durgaprasadarao, P.S. Sundar, S.H. Ahammad, M.M.A. Eid, Y. Lee, A.N.Z. Rashed, J.-Y. Ryu, *Dual features, compact dimensions and X-band applications for the design and fabrication of annular circular ring-based crescent-moon-shaped microstrip patch antenna*, Micromachines, **15**, *7*, pp. 1–13 (2024).
8. A.Z. Golubović, M.M. Ilić, *X-band series-fed microstrip patch antenna array*, Proc. 29th Telecommun. Forum (TELFOR), Belgrade, Serbia, pp. 1–4 (2021).
9. K. Malaisamy, M. Wasim, P. Sivagamasundhari, G. Sivakannu, V. Dinesh, *Array antenna design and development for X-band applications*, Computer Aided Constellation Management and Communication Satellites, Lecture Notes in Electrical Engineering, **987**, Springer, Singapore, pp. 1–10 (2023).
10. K. Sudhaman, T. Godhavari, R. Anusha, *Design of microstrip patch antenna at 10.3 GHz for X-band applications*, IOP Conf. Ser.: Mater. Sci. Eng., **993**, pp. 1–10 (2020).
11. T. Sarkar, A. Ghosh, L.L.K. Singh, S. Chattopadhyay, C.-Y.-D. Sim, *DGS-integrated air-loaded wideband microstrip antenna for X- and Ku-band*, IEEE Antennas and Wireless Propagation Letters, **19**, *1*, pp. 114–118 (2020).
12. L. Leszkowska, M. Rzymowski, K. Nyka, L. Kulas, *High-gain compact circularly polarized X-band superstrate antenna for CubeSat applications*, IEEE Antennas and Wireless Propagation Letters, **20**, *11*, pp. 2090–2094 (2021).
13. D. Samantaray, S.K. Ghosh, S. Bhattacharyya, *Modified slotted patch*

antenna with metasurface as superstrate for dual-band applications, IEEE Antennas and Wireless Propagation Letters, **22**, *1*, pp. 109–113 (2022).

14. A. Kumar, M. Kumar, A.K. Singh, *On the behavior of self-triplexing SIW cavity backed antenna with non-linear replicated hybrid slot for C and X-band applications*, IEEE Access, **10**, pp. 22952–22959 (2022).
15. S. Shankar, D.K. Upadhyay, *A fractal monopole antenna with dual polarization reconfigurable characteristics for X-band applications*, IEEE Access, **11**, pp. 95667–95680 (2023).
16. B.A. Nunna, V.K. Kothapudi, *A novel C/X-band linear polarized conformal shared aperture antenna array for spaceborne SAR applications*, IEEE Access, **11**, pp. 101045–101054 (2023).
17. P.M. Paul, K. Kandasamy, M.S. Sharawi, *A triband circularly polarized strip and SRR-loaded slot antenna*, IEEE Trans. Antennas Propag., **66**, *10*, pp. 5569–5573 (2018).
18. D. Gopinath, P. Marichamy, *On the design and analysis of multi-band microstrip patch antenna for wireless body area network applications*, J. Wireless Com. Network, **2025**, *13*, pp. 1–10 (2025).
19. M.Z. Baba-Ahmed, R.D. Taleb, M.A. Rabah, S. Benabbou, M.I. Soufi, *Hybrid design patch antenna for X-band satellite communication*, Rev. Roum. Sci. Techn. – Électrotechn. et Énerg., **70**, *3*, pp. 379–384 (2025).
20. C.A. Balanis, *Antenna theory: Analysis and design*, 4th ed., Wiley, pp. 783–858 (2016).
21. B.S. Virdee, T. Aribi, T. Sedghi, *Dual-band multi-layer antenna array with circular polarization and gain enhancement for WLAN and X-band applications*, Micromachines, **16**, pp. 1–12 (2025).
22. A. Suresh, V. Karteek, C. Ravikumar, C. Dhanamjayulu, K. Tai-hoon, S. Kumar, *Meta-atom loaded circularly polarized triple band patch antenna for Wi-Fi, ISM and X-band communications*, Heliyon, **10**, *7*, pp. 1–13 (2024).